Spiral turbulence developed through the formation of superimposed target waves in an oscillatory reaction-diffusion medium

Lu Zhang,[1] Qingyu Gao,[1,*] Qun Wang,[1] Hai Wang,[1] and Jichang Wang[1,2,†]
[1]*College of Chemical Engineering, China University of Mining and Technology, Xuzhou 221008, People's Republic of China*
[2]*Department of Chemistry and Biochemistry, University of Windsor, Ontario, Canada, N9B 3P4*
(Received 26 March 2006; revised manuscript received 28 July 2006; published 17 October 2006)

An approach leading to the development of spiral turbulence is reported here in an oscillatory reaction-diffusion medium, which is through the spontaneous formation of targetlike waves near the core of a spiral wave. The newly formed target wave emerges with its own characteristic frequency and propagates on top of the original spiral wave, which eventually leads to the breakup of the spiral at a location far from the spiral center. The radius of the surviving spiral segment decreases rapidly with the bifurcation control parameter. Calculation of power spectra suggests that the meandering of the spiral tip is responsible for the onset of the superimposed target and the phase desynchronization of the superimposed target waves.

DOI: 10.1103/PhysRevE.74.046112 PACS number(s): 82.20.Wt, 05.40.−a, 47.27.Cn, 82.40.Ck

I. INTRODUCTION

Spiral waves have been observed in a variety of systems in nature ranging from physical to biological media such as fluid systems [1], premixed flames [2], the Belousov-Zhabotinsky (BZ) reaction [3,4], catalytic reactions on platinum surface [5], the glycolysis in the yeast extract [6], aggregating starving slime mold cells [7], the cardiac tissue [8], and cellular calcium release [9]. Many types of spiral wave activities such as superarmed [10], ripplearmed [11], zigzagarmed [12], multiarmed [13], and segmented spirals [14,15] have been reported in the past two decades.

In addition to investigations on spiral formation, the transition from a regular spiral to spiral turbulence has also attracted a great deal of attention from both experimental and theoretical researchers. It is partially driven by the fact that understanding the formation of defect-mediated spiral turbulence has profound potential applications. Spiral turbulences, for example, have been found to cause fibrillation in the heart [16], which has severe impacts on quality of life. Doppler instability induced by the meandering of the spiral tip has been suggested to be responsible for the breakup of spirals in excitable media [17,18]. In spatially extended oscillatory systems, spirals could break up either via the formation of a superstructure due to long-wavelength modulations [18–20], or by the transverse instability of the line defects of the period-2^n spiral waves [21,22]. In this study, transitions of regular spirals to spiral turbulence were investigated in an oscillatory reaction-diffusion medium exhibiting complex temporal oscillations, and a new scenario was found.

II. MODEL

The model employed in this research was developed by Decroly and Goldbeter in 1982 to analyze enzyme reaction kinetics [23]. Equations of the reaction-diffusion system read

$$\frac{\partial \alpha}{\partial t} = (\upsilon/K_{m1}) - \sigma_1 \Phi + D\nabla^2 \alpha,$$

$$\frac{\partial \beta}{\partial t} = q_1 \sigma_1 \Phi - \sigma_2 \eta + D\nabla^2 \beta,$$

$$\frac{\partial \gamma}{\partial t} = q_2 \sigma_2 \eta - k_s \gamma + D\nabla^2 \gamma \tag{1}$$

with

$$\Phi = \alpha(1+\alpha)(1+\beta)^2/[L_1 + (1+\alpha)^2(1+\beta)^2]$$

and

$$\eta = \beta(1+d\beta)(1+\gamma)^2/[L_2 + (1+d\beta)^2(1+\gamma)^2], \tag{2}$$

where variables α, β, and γ represent three biochemical species. Parameters υ, K_{m1}, σ_1, σ_2, q_1, q_2, L_1, L_2, d, and k_s are determined by reaction conditions. Detailed discussions on the above model can be found in Ref. [23]. Diffusion coefficients of all three species, denoted by D, are set equal in this study. In the absence of transportations, the above model can support various complex temporal dynamics, including birhythmicity, hard excitation, and chaos as the control parameter k_s is varied. This study focuses on the conditions in which the system exhibits bursting oscillations. As in earlier studies [23], k_s is investigated as the control parameter. Calculations were carried out with the Euler integration method with a space grid $dx=dy=0.002$ cm and an integration time step $dt=0.02$ s. Diffusion coefficients used in our simulation are equal to 1.0×10^{-6} cm^2 s^{-1}. The space measurement and diffusion coefficients are not normalized in this study. Therefore, these numbers appear to be much larger than those seen in the simulations of the BZ model in which normalization has been implemented [3]. Nonflux boundaries were used in the following simulations. When spatial grids and time steps were reduced to half of the values used here, the same results as shown in the following were obtained. We also examined the results with the Runge-Kutta method, and the same results were achieved.

*Electronic address: gaoqy@cumt.edu.cn
†Electronic address: jwang@uwindsor.ca

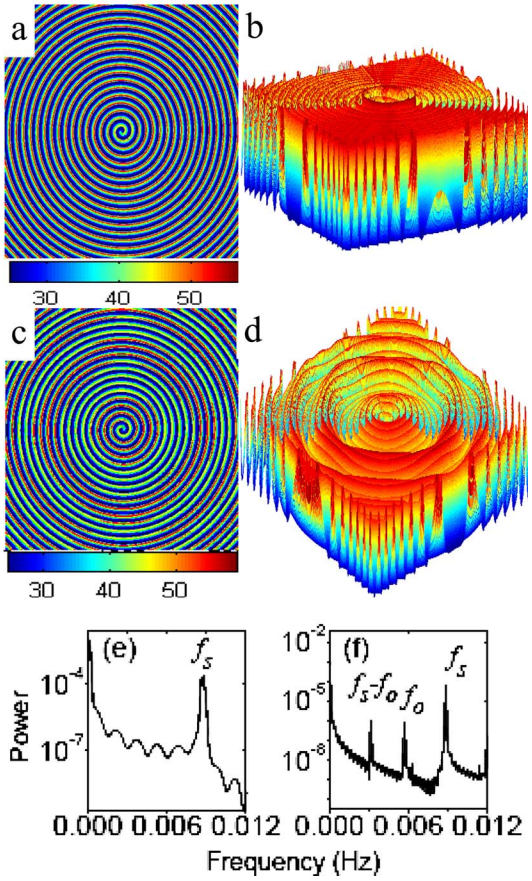

FIG. 1. (Color online) Superimposed target waves collected at different time when $k_s=2.502\ s^{-1}$: (a) 4000 s and (c) 24 000 s. (b) and (d) are the corresponding concentration profiles of (a) and (c). Variable α plotted in this figure. (e) and (f) are the power spectra of simple and modulated spirals calculated, respectively, at (e) $k_s=2.55\ s^{-1}$ and (f) $k_s=2.502\ s^{-1}$. Other parameters are $\upsilon/K_{m1}=0.45\ s^{-1}$, $\sigma_1=\sigma_2=10.0\ s^{-1}$, $q_1=50.0$, $q_2=0.02$, $L_1=5.0\times10^8$, $L_2=100.0$, $d=1.0\times10^{-6}\ cm^2\ s^{-1}$, and $D=1.0\times10^{-6}\ cm^2\ s^{-1}$. The size of the system shown in panels (a)–(d) is 1200×1200 grids.

III. THE FORMATION OF SUPERIMPOSED TARGET WAVES

For k_s larger than $2.55\ s^{-1}$, the above reaction-diffusion medium supports a simple spiral wave that has the same amplitude everywhere except within the neighborhood of the spiral tip. As the control parameter k_s decreases, the simple spiral becomes unstable and its local amplitude begins to oscillate. The modulation starts from the core of the spiral wave and then propagates outward, leading the formation of targetlike waves in the medium shown in Fig. 1. Figures 1(a) and 1(b) illustrate the onset of the targetlike wave around the spiral center, whereas Figs. 1(c) and 1(d) present the subsequent propagation of the target wave. After the appearance of the target wave, the initial spiral is still there [see Figs. 1(a) and 1(c)], therefore the newly developed targetlike patterns are called superimposed target waves in this study.

Figure 1(e) is the power spectrum of a simple spiral calculated at $k_s=2.550\ s^{-1}$. This power spectrum demonstrates that local oscillations of a simple spiral have only one frequency at $f_s=0.008\ 77$ Hz. Figure 1(f) presents the power spectrum of local oscillations collected at a point far from the spiral tip in Fig. 1(c). In contrast to a single peak seen in Fig. 1(e), three major peaks are obtained in Fig. 1(f), which are the frequencies of the spiral wave ($f_s=0.008\ 77$ Hz), the overtargets ($f_o=0.005\ 72$ Hz), and the difference of f_s-f_o (at 0.003 05 Hz), respectively. Notably, the formation of the overtarget wave does not alter the frequency of the initial spiral.

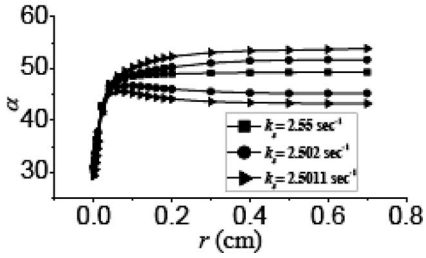

FIG. 2. The highest and lowest crest of local oscillations plotted against a spatial coordinate. All other parameters used in this calculation are the same as those used in Fig. 1.

From Fig. 1(c), one can see that the wavelength of superimposed target waves is more than four times larger than that of the spiral, implying that the above observed spiral instability is of a long-wavelength type. However, different from what was seen in earlier reports [18–20], in which the long-wavelength instability resulted in periodic variations in spiral wavelength and the formation of superspirals, here the long-wavelength instability results mainly in modulations in the amplitude of the spiral. There is barely any modulation in the spiral wavelength. Such a conclusion is derived based on calculations of the spatial power spectra, which illustrate that the wave number of a modulated spiral wave such as the one shown in Fig. 1(c) is the same as that of a simple spiral (both have a reading at $13.672\ cm^{-1}$). As the control parameter k_s decreases, the wavelength and frequency of the above observed superimposed target waves increases.

IV. MODULATIONS IN THE AMPLITUDE AND MOTION OF THE SPIRAL TIP

Figure 2 plots variations of spiral amplitudes as a function of the distance from the spiral center, in which for clarity only values of the highest and lowest magnitude of the local oscillations are plotted. Three dynamic conditions are investigated here, which correspond to $k_s=2.550$, 2.502, and $2.5011\ s^{-1}$, respectively. As is shown in the figure, there is no modulation in the spiral amplitude near the spiral tip. For a stable spiral, there is no modulation in its amplitude throughout the medium, whereas modulation in the spiral amplitude is enhanced as k_s decreases. Meanwhile, the magnitude of the modulation appears to increase with the distance from the spiral core. Thus, results in Fig. 2 show the convective property of the modulation, in which the modulation of the spiral amplitude increases as it moves away from the spiral tip. We would like to point out that data plotted here are only the largest and the smallest amplitudes of the corresponding local oscillations. Details of these local oscillations (i.e., the

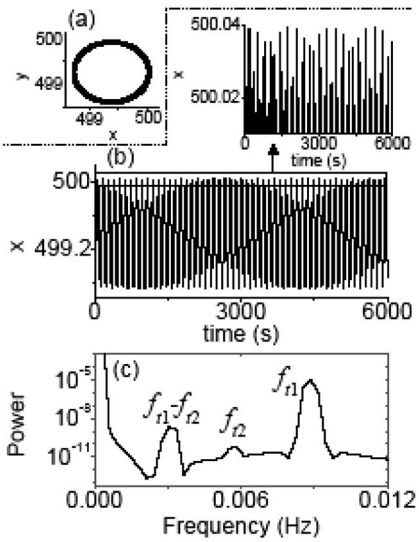

FIG. 3. (a) Trajectories of the spiral tip; (b) plot of the horizontal location of the spiral tip as a function of time; and (c) a power spectrum calculated from the oscillations shown in (b). The reaction dynamics corresponds to k_s=2.502 s^{-1}.

oscillation mode) may be different from each other, depending on the k_s value. Such a dependence is characterized in the following simulations.

Our analysis shows that for the simple spiral, its tip moves along a perfect circle. The motion of the tip alone the horizontal direction has a unique frequency that is equal to the spiral frequency (0.008 77 Hz). When the temporal reaction dynamics is adjusted by decreasing k_s, the spiral tip begins to meander, generating a thick circle over time [shown in Fig. 3(a)]. Figure 3(b) is the plot of the x coordinate of the spiral tip versus time, which resembles torus oscillations seen in various nonlinear systems. Remarkably, Fig. 3(c) shows that the motion of the spiral tip has a second frequency f_{t2}, which is identical to the frequency of the superimposed target wave, f_o. Together with the observation that superimposed target waves do not occur until the spiral meandering behavior occurs, the above results suggest that spiral meandering is responsible for the spontaneous formation of the superimposed targets. The tip meandering becomes more serious as k_s decreases. However, despite the fact that the tip meandering becomes more serious as k_s decreases, the motion of the spiral tip is always confined within a very small region. For example, the radius is 0.001 31 cm for a simple spiral (k_s=2.55 s^{-1}) and is merely increased to 0.001 41 cm for k_s=2.50 s^{-1}. As a result, there is barely any modulation in the spiral wavelength during the above changes.

V. TRANSITION FROM A SIMPLE SPIRAL TO SPIRAL TURBULENCE

The spatial structure shown in Fig. 1(d) illustrates that variations in the local amplitude of the overtarget wave along its circumference are not synchronized. The degree of such phase desynchronization increases as k_s is decreased. The

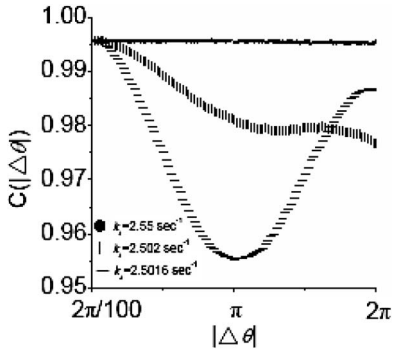

FIG. 4. Correlation functions of the local oscillations at points along the spiral arm. All parameters used in this calculation are the same as those used in Fig. 1.

phase desynchronization is quantified by calculating values of the correlation function $C(|\Delta\theta|)$ between the oscillations of two local points with a $\Delta\theta$ angle difference along the same spiral arm, and the calculated results are presented in Fig. 4. As is shown in this figure, for a simple spiral wave (k_s =2.55 s^{-1}), $C(|\Delta\theta|)$ is constant with the increase of $|\Delta\theta|$. It is consistent with the fact that the local dynamics of the points on the simple spiral arm are synchronized in phase. However, for a well-defined overtarget wave at k_s =2.502 s^{-1}, C($|\Delta\theta|$) decreases with respect to an increase of $|\Delta\theta|$. The decrease in C($|\Delta\theta|$) values implicates the occurrence of phase desynchronization along the spiral arm, which subsequently causes the superimposed target wave to become irregular. As k_s is further decreased to 2.5016 s^{-1}, the $C(|\Delta\theta|)$ value at the same $|\Delta\theta|$ is further reduced, indicating that decreasing k_s causes the superimposed target to become more and more irregular. Eventually, the breakup of the stable superimposed target wave takes place when k_s crosses a threshold value ($\leqslant$2.5016 s^{-1}).

Figure 5 presents wave activities under different dynamic conditions, k_s: (a) 2.55 s^{-1}, (b) 2.502 s^{-1}, (c) 2.500 s^{-1}, (d) 2.498 s^{-1}, and (e) 2.300 s^{-1}. Only a simple, stable spiral is observed in Fig. 5(a), whereas both spiral and superimposed target waves are achieved in Fig. 5(b). Figures 5(c) and 5(d) show the coexistence of a stable spiral core and spiral fragments. As a result of further decreasing k_s in Fig. 5(e), the whole medium is dominated by spiral turbulence. Temporal dynamics of the homogeneous system under the conditions used in Figs. 5(a)–5(d) are all similar, exhibiting burst oscillations as shown in Fig. 5(f). Since there is no qualitative change in the temporal dynamics in Fig. 5, the coupling with diffusion transportations plays an important role in leading the transition from a simple spiral to spiral turbulence.

In the case in which spiral turbulence is not fully developed, such as the ones shown in Figs. 5(c) and 5(d), power spectra of local oscillations illustrate that there are three distinct dynamic regions: (i) a large spiral segment in the center of the system, in which the spiral fragment still has two independent frequencies, e.g., the frequency of the original spiral (0.008 77 Hz) and the frequency of the overtarget (0.006 01 Hz) [see Fig. 6(a)]; (ii) the turbulent area, where the local dynamics are chaotic with a major frequency labeled f_b (0.008 77 Hz) [see Fig. 6(b)]; and (iii) an area out-

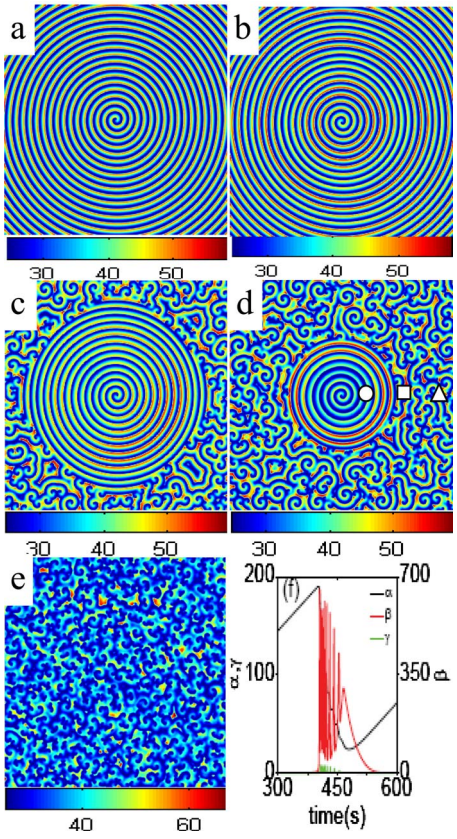

FIG. 5. (Color online) Wave activities at different k_s values: (a) 2.55 s^{-1}, (b) 2.502 s^{-1}, (c) 2.500 s^{-1}, (d) 2.498 s^{-1}, and (e) 2.3 s^{-1}. (f) is the temporal dynamics of the homogeneous system when k_s =2.55 s^{-1}. Other parameters used here can be found from Fig. 1.

side of region (ii), where despite the fact that the pattern has no obvious difference from region (ii), only one frequency in the power spectrum that is equal to the frequency of the original spiral is obtained there [see Fig. 6(c)].

Figure 7 shows the process of spiral breakups, which is conducted by adjusting k_s from 2.502 s^{-1} directly to 2.495 s^{-1} at the beginning of the simulation. Figures 7(a) and 7(b) illustrate that shortly after the change of k_s, the superimposed target becomes desynchronized along its circumference. The severely desynchronized superimposed target waves gradually induce the breakup of the original spiral at a

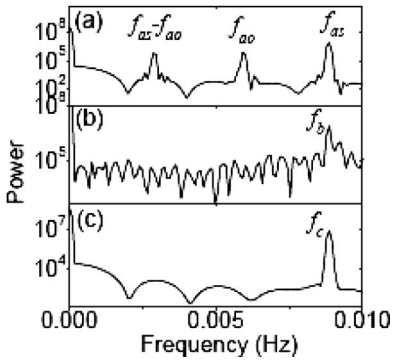

FIG. 6. Power spectra of the local oscillations collected at the points shown in Fig. 4(d): (a) circle, (b) square, and (c) triangle.

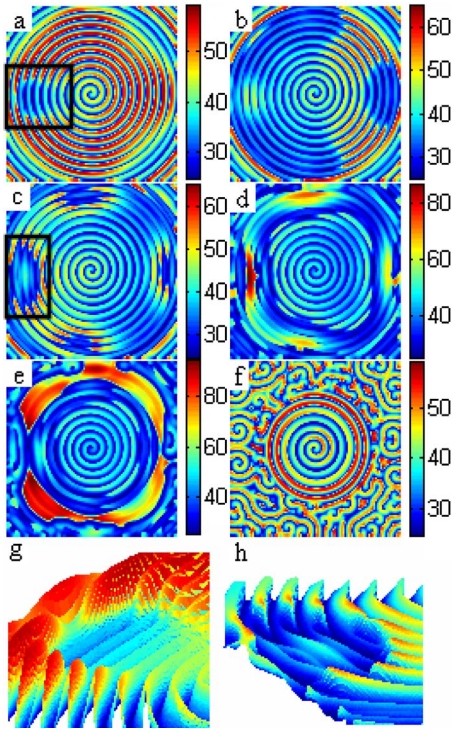

FIG. 7. (Color online) Snapshots showing the development of spiral breakups when k_s is varied from 2.502 s^{-1} directly to 2.495 s^{-1}: (a) t=2100 s; (b) t=2300 s, (c) t=2500 s, (d) t=2700 s, (e) t=2900 s, (f) t=10 000 s. (g) and (h) are the three-dimensional concentration profiles of the two portions outlined in panels (a) and (c).

place far from the spiral core, where modulations in the spiral amplitude are larger [see Figs. 7(c)–7(e)]. Three-dimensional concentration profiles in Figs. 7(g) and 7(h) illustrate the desynchronization of the superimposed target wave and the breakup of the spiral. Eventually, the system evolves to a stable situation shown in Fig. 7(f), in which a large segment of the initial spiral is preserved. Variations of the time-averaged radius r_s of the remaining spiral segment are plotted in Fig. 8 as a function of k_s, which shows that the size of the surviving spiral decreases rapidly as soon as the dynamics allows spiral breakups to take place and the process of the size decrease with the decrease of k_s appears to

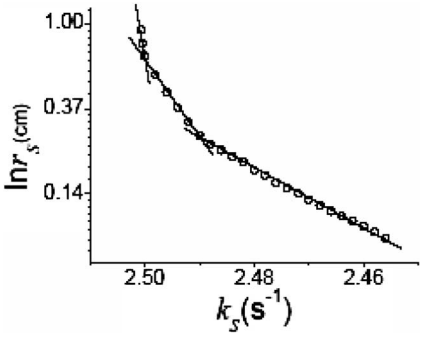

FIG. 8. Radius r_s of the stable spiral fragment as a function of k_s. The size of the reaction-diffusion medium is 800×800 grids. Other parameters are the same as those used in Fig. 1.

have three stages according to the difference in their exponent value. To test the robustness of the above results, we have increased the size of the medium by 50% (i.e., with 1200×1200 grids) under the condition $k_s=2.498\ s^{-1}$, and the actual size of the remaining stable spiral is found to the same as the one shown in Fig. 5(d) where 800×800 grids are used.

VI. SUMMARY

Earlier studies illustrate that spiral breakups may take place as a result of the neighboring two spiral fronts becoming so close to each other that the local wavelength is beyond the critical value allowed by the dispersion relation [17–20,24,25]. Through spatial Fourier analysis, we found that in this study the spiral wavelength remains nearly constant in the process of spiral breakup, implicating that a new mechanism is responsible for the development of spiral turbulence here. Our simulations suggest that it arises from the coupling of two factors: (i) the desynchronization of the superimposed target along its circumference, and (ii) modulation in spiral amplitude that increases gradually while moving away from the spiral core. Presumably, the appearance of superimposed target waves arises from the torus meandering of the spiral tip as they have the same frequency. A similar scenario has been obtained when periodic boundaries are used.

A unique feature of this three-variable Decroly-Goldbeter model is that there are two nonlinear feedback loops internally coupled together. From a dynamic point of view, a system with coupled feedback loops can also be achieved through imposing an external periodic or constant forcing. Therefore, results obtained in this study may be valid to externally coupled reaction-diffusion media.

ACKNOWLEDGMENTS

This work was supported through NSFC (Grant No. 20573134), RFDP (Grant No. 20050290512), and NCET (Grant No. 05-0477) of China. We acknowledge the help of Dr. Lingfa Yang (Brandeis University) in our computation. J. W. would like to thank CUMT and NSERC for financial support.

[1] M. C. Cross and P. C. Hohenberg, Rev. Mod. Phys. **65**, 851 (1993).
[2] S. K. Scott, J. C. Wang, and K. Showalter, J. Chem. Soc., Faraday Trans. **93**, 1733 (1997).
[3] A. T. Winfree, Science **175**, 634 (1972).
[4] *Chemical Waves and Patterns*, edited by R. Kapral and K. Showalter (Kluwer Academic Publishers, Dordrecht, 1995).
[5] M. Bertram, C. Beta, M. Pollmann, A. S. Mikhailov, H. H. Rotermund, and G. Ertl, Phys. Rev. E **67**, 036208 (2003).
[6] T. Mair and S. C. Muller, J. Biol. Chem. **271**, 627 (1996).
[7] K. J. Lee, E. C. Cox, and R. E. Goldstein, Phys. Rev. Lett. **76**, 1174 (1996).
[8] S. Hwang, T. Y. Kim, and K. J. Lee, Proc. Natl. Acad. Sci. U.S.A. **102**, 10363 (2005).
[9] J. Lechleiter, S. Girard, E. Peralta, and D. Clapham, Science **252**, 123 (1991).
[10] V. Perez-Munuzuri, R. Aliev, B. Vasiev, V. Perez-Villar, and V. I. Krinsky, Nature (London) **353**, 740 (1991).
[11] M. Markus, G. Kloss, and I. Kusch, Nature (London) **371**, 402 (1994).
[12] Y. A. Astrov, I. Muller, E. Ammelt, and H.-G. Purwins, Phys. Rev. Lett. **80**, 5341 (1998).
[13] K. Agladze and V. I. Krinsky, Nature (London) **296**, 424 (1982).
[14] V. K. Vanag and I. R. Epstein, Proc. Natl. Acad. Sci. U.S.A. **100**, 14635 (2003).
[15] L. Yang, I. Berenstein, and I. R. Epstein, Phys. Rev. Lett. **95**, 038303 (2005).
[16] F. X. Witkowski *et al.*, Nature (London) **392**, 78 (1998).
[17] M. Bär and M. Eiswirth, Phys. Rev. E **48**, R1635 (1993).
[18] L. Q. Zhou and Q. Ouyang, J. Phys. Chem. A **105**, 112 (2001).
[19] Q. Ouyang and J. M. Flesselles, Nature (London) **379**, 143 (1996).
[20] L. Q. Zhou and Q. Ouyang, Phys. Rev. Lett. **85**, 1650 (2000).
[21] A. Goryachev, H. Chate, and R. Kapral, Phys. Rev. Lett. **80**, 873 (1998).
[22] J. S. Park, S. J. Woo, and K. J. Lee, Phys. Rev. Lett. **93**, 098302 (2004).
[23] O. Decroly and A. Goldbeter, Proc. Natl. Acad. Sci. U.S.A. **79**, 6917 (1982).
[24] M. Bär and M. Or-Guil, Phys. Rev. Lett. **82**, 1160 (1999).
[25] M. Bär and L. Brusch, New J. Phys. **6**, 5 (2004).